

Millimeter Wave Multi-mode Transmission Line Components

Gregory G. Denisov · Alexey V. Chirkov · Vladimir I. Belousov · Alexander A. Bogdashov · Galina I. Kalynova · Dmitry I. Sobolev · Yury V. Rodin · Evgeny M. Tai · Vladimir I. Ilin · Sergey Yu. Kornishin · Maxim L. Kulygin · Vladimir I. Malygin · Elena A. Soluyanova · Vladimir V. Parshin · Michael Yu Shmelev

Received: 29 November 2010 / Accepted: 3 December 2010 /
Published online: 11 January 2010
© Springer Science+Business Media, LLC 2011

Abstract The present paper reports on the recent development of several oversized millimeter wave transmission line components for different applications. The studies include a circular TE_{11} -to-Gaussian beam mode converting horn, a TM_{01} -to-rotating TE_{31} mode converter, a TE_{11} -mode 90° bend, a series of different HE_{11} -mode transmission line components, a notch filter and a fast laser controlled semiconductor microwave switch.

Keywords Oversized transmission lines · Mode converters · Bends · HE_{11} mode components · Notch filters · Semi-conductor microwave switches

1 Introduction

Multi-mode components are often used for transmission and control of millimeter waves [1–3]. For example, large, comparing with wavelength, component sizes are absolutely mandatory for high-power millimeter waves in gyrotron-based electron-cyclotron-wave (ECW) systems of thermonuclear plasma fusion installations.

The IAP has long term (~50 years) experience in the development and use of quasi-optical (QO) and multi-mode systems. Basic principles were formulated in the 1960s–70s in papers of V.I.Talanov, M.I.Petelin, N.F. Kovalev, S.N.Vlasov: General features of QO beam propagation, integral equations (Maxwell, parabolic), scalings of similar solutions,

G. G. Denisov (✉) · A. V. Chirkov · V. I. Belousov · A. A. Bogdashov · G. I. Kalynova · D. I. Sobolev · Y. V. Rodin · S. Y. Kornishin · M. L. Kulygin · V. I. Malygin · V. V. Parshin · M. Y. Shmelev
Institute of Applied Physics (IAP), RAS, Nizhny Novgorod, Russia
e-mail: den@appl.sci-nnov.ru

E. M. Tai · E. A. Soluyanova
GYCOM Ltd, Nizhny Novgorod, Russia

V. I. Ilin
Tokamak Physics Institute of RRC “Kurchatov Institute”, Moscow, Russia

principles of mode selection, optimal transmission through apertures, rippled mode converters for multi-mode waveguides, QO converters of high-order modes into paraxial wave beams, and others.

The components developed at IAP/GYCOM operate at frequencies in the range centimeter, millimeter and sub-millimeter wavelengths with different powers. For example, for ECW systems a typical frequency is in the range of 70–170 GHz and power per unit comparable with 1 MW in pulses of 0.1 ...1000 seconds. The microwave components often used here are: matching optics, barrier windows, directional couplers, switches, loads, waveguides, mirrors, polarizers, DC-breaks, mode filters, pumping ports, and bellows. Relativistic microwave electronics devices operate with power comparable with 1 GW in short pulses 1...100 ns. In contrast there are very low power applications like plasma diagnostics ($P \sim 10^{-9} - 10^{-3}$ W). Of course there also are medium power (10 W—10 kW) application as radars, technology (ceramics, CVD plasmas, ion sources, *etc.*), and Dynamic Nuclear Polarization (DNP) Nuclear Magnetic Resonance (NMR) spectroscopy.

We also can note in the introduction more recent and world recognized methods/approaches for multi-mode systems developed at IAP (the year of first publication is shown): measurement of QO beams by infrared camera (1990), effective conversion of gyrotron operating modes into eigenmodes of open transmission lines (1991), use of the Talbot effect for microwave systems (1992), use of iterative QO mirror synthesis (1993), iterative method of phase retrieval from intensity measurements (1994), one- and two-dimensional Bragg reflectors for microwaves (1982, 1998), optimal waveguide multi-mode converter synthesis (2004), measurement of low-loss material microwave properties (1980), high-power microwave pulse compressors (2000), waveguide gaps/miter bends with minimum losses (2005), fast directional switch—FADIS (2007).

This paper does not pretend to be an overview of all approaches in calculation and design of multi-mode components or description of all technical details. It just includes a few different “fresh” examples in the field:

- General principles of waveguide converters,
- Transmission line at Kurchatov Institute gyrotron test stand,
- 258 GHz transmission line for DNP,
- High-suppression notch filters,
- Fast laser controlled semiconductor microwave switch.

1.1 Principles of waveguide surface synthesis

Multi-mode waveguide synthesis can be formulated on the base of three principles [4–6] listed below (A–C):

- A. *The deformation of the waveguide surface at each iteration step is defined by two field distributions calculated using boundary conditions at the input and output of the waveguide:* Let us consider a waveguide unit (Fig. 1) with the given input cross-section S_1 , output cross-section S_2 , electric and magnetic fields at the both cross-sections (E_1 and H_1 at the input, and E_2 and H_2 at the output, respectively). The initial waveguide surface is denoted S_0 and the time dependence is taken as $\exp(-i\omega t)$. Two field distributions are calculated inside the waveguide by some field analysis method. The first one is calculated by using the input field and the second one, by using the spatially reversed output field ($\vec{E}_{-2} = \vec{E}_2^*$, $\vec{H}_{-2} = -\vec{H}_2^*$, the asterisk stands for complex conjugation) as a boundary condition. The fields inside the waveguide are denoted

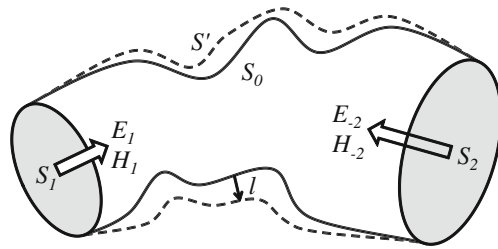


Fig. 1 Explanation of main notations: two given waveguide cross-sections S_1 and S_2 (input and output, respectively), the non-deformed waveguide surface S_0 (before iteration) and the deformed surface S' (after iteration), the deformation amplitude l at some point of the surface, the specified input fields E_1 and H_1 , and the desired output fields E_{-2} and H_{-2} . The negative signs in the second pair of the fields mean that they were spatially reversed.

later in the same way as the corresponding fields in the cross-sections. Assuming that the conversion is complete, these two field distributions are equal to each other or differ only by the constant phase multiplier $\exp(i\varphi_0)$.

The initial waveguide surface does not ensure 100% conversion of the input field to the output one. To improve the conversion efficiency, we will deform the waveguide surface slightly at each iteration step in such a way that the conversion efficiency is increased by a specified value. Here, “slightly” means that the deformation amplitude is small enough to satisfy the following equivalent boundary condition discussed in detail in [3]:

$$\vec{E} \vec{\tau} = \vec{\tau} \text{grad}(E_n l) - ikl [\vec{n} \times \vec{H}] \vec{\tau}, \tag{1}$$

where $\vec{\tau}$ is the unit tangent vector to S_0 , \vec{n} is the external unit normal vector to S_0 , and l is the deformation amplitude (distance between S_0 and S' , which is positive when S' is on the outside). Equation 1 describes the equivalence between deformation of the conducting surface and introduction of a tangential electric field (or a current source) on the non-deformed surface. The equation is satisfied only when the deformation amplitude l at a single iteration step is much smaller than the wavelength λ . The distance between the initial surface and the final synthesized surface of the waveguide does not have to be small, because the fields are recalculated for the new surface at each iteration step.

B. *The deformation satisfies the integral equation written for a specific field representation:* Several analysis methods are commonly used to calculate the fields inside a waveguide depending on the deformation type and the waveguide size-to-wavelength ratio. Different methods may use different types of field representation (e.g. field components, surface currents or mode amplitudes), and to avoid conversion-related problems and a possible decrease in the calculation speed, the method of synthesis must fit the field analysis method precisely. Let us write the integral equation for the field components. Applying Lorentz’s lemma to calculated field distributions and assuming that deformation satisfies (1), we get the 1st-order (in terms of the deformation amplitude-to-wavelength ratio) estimate of the increase in the waveguide conversion efficiency after a slight deformation:

$$\Delta P = \int_{S_0} l F dS, \quad F = -ik(\vec{H}_{\tau 1} \vec{H}_{\tau -2} + E_{n 1} E_{n -2}). \tag{2}$$

where ΔP is the differences of mutual powers after and before the iteration (both field distributions are normalized in such way that the total transmitted power is equal to unity). A similar integral equation can be written for any type of field representation.

C. *The solution of the integral equation is found in accordance with the restrictions imposed on the waveguide deformation.* Each of (2) and similar integral equations written for other field representations has a set of solutions for the chosen ΔP , and we have to find an optimal one in accordance with certain criteria. In the simplest case, there are no additional constraints and we choose the solution with the minimal Euclidean norm. The function l is real, therefore, we rewrite (2) as two real equations. Writing the first variation with Lagrange multipliers and solving the system of equations, we find the solution:

$$l = \alpha \text{Re}F + \beta \text{Im}F, \tag{3.1}$$

$$\alpha = \frac{N_{\text{Im}} \text{Re} \Delta P - N_{\text{ReIm}} \text{Im} \Delta P}{N_{\text{Re}} N_{\text{Im}} - N_{\text{ReIm}}^2}, \tag{3.2}$$

$$\beta = \frac{N_{\text{Re}} \text{Im} \Delta P - N_{\text{ReIm}} \text{Re} \Delta P}{N_{\text{Re}} N_{\text{Im}} - N_{\text{ReIm}}^2},$$

$$N_{\text{Re}} = \int_{S_0} |\text{Re}F|^2 dS \quad N_{\text{Im}} = \int_{S_0} |\text{Im}F|^2 dS, \tag{3.3}$$

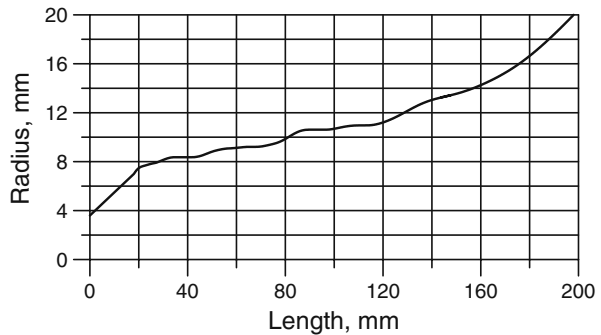
$$N_{\text{ReIm}} = \int_{S_0} \text{Re}F \text{Im}F dS.$$

To synthesize waveguide units with specified additional specified properties, other methods are constructed. If smoother solutions are needed, then the norm of the two-dimensional gradient is minimized. Fulfillment of geometrical constraints can also be incorporated in the method by adding the corresponding equations in the system. Fulfillment of the restrictions during the main synthesis procedure eliminates interference of the conservation routine with the convergence and stability at a very small computational cost.

New methods of synthesis have been derived from these principles. Several tens of waveguide mode converters, tapers and bends with unique parameters were synthesized and tested already. To illustrate the performance of the new methods we present only three examples.

- 1) A smooth wall circular waveguide taper converting the TE_{11} mode into a Gaussian beam (Fig. 2). The frequency is 95 GHz, the length 198 mm, the diameter increases from 3.6 mm at the input to 40 mm at the output. The beam width is smaller than usual (7.464 mm instead of 9.12 mm) therefore it is represented as a 4-mode mixture containing 71.9% TE_{11} , 23.4% TM_{11} , 4.4% TE_{12} and 0.3% TM_{12} . The calculated efficiency is over 99.5%, and the measured efficiency is over 99%.
- 2) A waveguide mode converter from the TM_{01} mode to the rotating TE_{31} mode. The central frequency is 9.75 GHz, the calculated efficiency is over 99% at 9.75 GHz and over 95%, at a bandwidth of 0.5 GHz. The measured efficiency is over 98% at the central frequency and over 92%, in the whole 0.5 GHz band. A simulated view of the waveguide mode converter surface is shown on Fig. 3.

Fig. 2 Profile of the circular waveguide taper converting the TE_{11} mode into a Gaussian beam.



- 3) A wideband 90-degree waveguide bend conserving the TE_{11} mode. The total bend length along the axis is 450 mm and the waveguide diameter is 32.6 mm. The calculated efficiency is over 98% in the broad frequency band 6...30 GHz and higher than 99% in the band 16...27 GHz (Fig. 4).

1.2 Transmission line at Kurchatov Institute gyrotron test stand

The line was designed for testing gyrotrons with power up to 1.5 MW in CW regime. So far the line itself was tested with maximum microwave parameters 1 MW/570 sec and 0.8 MW/1000 sec defined by the capabilities of the gyrotron.

The major components of the line operate in vacuum. They are:

- matching optics unit (graphite absorber, up to 5% power)
- 4 channel arc-detector protection
- bi-directional coupler, attenuator, detector (for monitor and interlock)
- 88 mm diam. corrugated HE_{11} waveguides
- switch between main vacuum CW load/ atmospheric pulse load, short pulse window
- CW load and pulse load (0.2 sec)
- pumping ports, cooling circuit

The line is in use approximately since two years. During this period there was no one serious complain operation of the line. A similar line is used at the GYCOM gyrotron test stand in Nizhny Novgorod. The pictures below (Fig. 5) illustrate the line performance.

More components of the line are shown on Fig. 6.

To absorb and measure megawatt power loads made of stainless steel are used. The microwaves are absorbed by a very large surface of metal pipes (without surface coating) with water cooling. There are two versions of such a load: the small one (size 0.6×1 m) with absorbing surface of 7 m^2 and reflection about 4% in the form of stray radiation; the big one (size 0.7×1.6 m) with absorbing surface of 17 m^2 . The small load was tested at maximum gyrotron parameters (1 MW/570 sec and 0.8 MW/100 sec). The big load probably can withstand at very high power up to 2–3 MW since for 2 MW power of

Fig. 3 Simulated surface of the waveguide mode converter from the TM_{01} mode to the rotating TE_{31} mode.

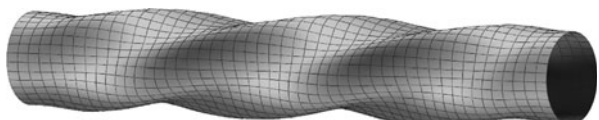
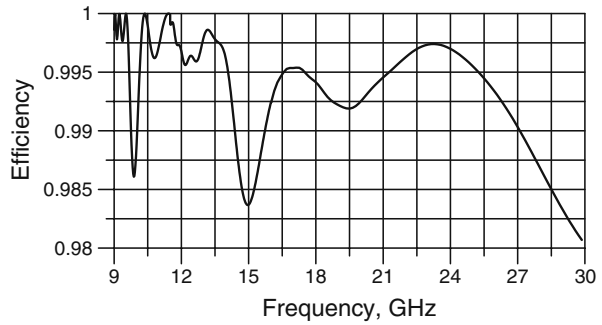


Fig. 4 Efficiency graph of 90-degree waveguide bend conserving the TE₁₁ mode.



microwaves the specific load on the absorbing pipe surface is only 12 W/cm² and temperature increase of the surface is only 20°. Some load details are shown in Fig. 7.

1.3 258 GHz transmission line for DNP-NMR spectroscopy

Dynamic nuclear polarization (DNP) is a nuclear magnetic resonance (NMR) technique utilized to enhance the polarization of the nuclei through irradiation of the electron spins by microwaves in the neighborhood of their Larmor frequency [7, 8]. To obtain higher resolution spectra, it is desirable to perform DNP at higher magnetic field strengths (9–18 T), where NMR is commonly employed today. There are several problems encountered when performing DNP at high fields. First, the enhancement decreases with increasing static field strength. Second, the relaxation mechanisms responsible for the DNP effect are

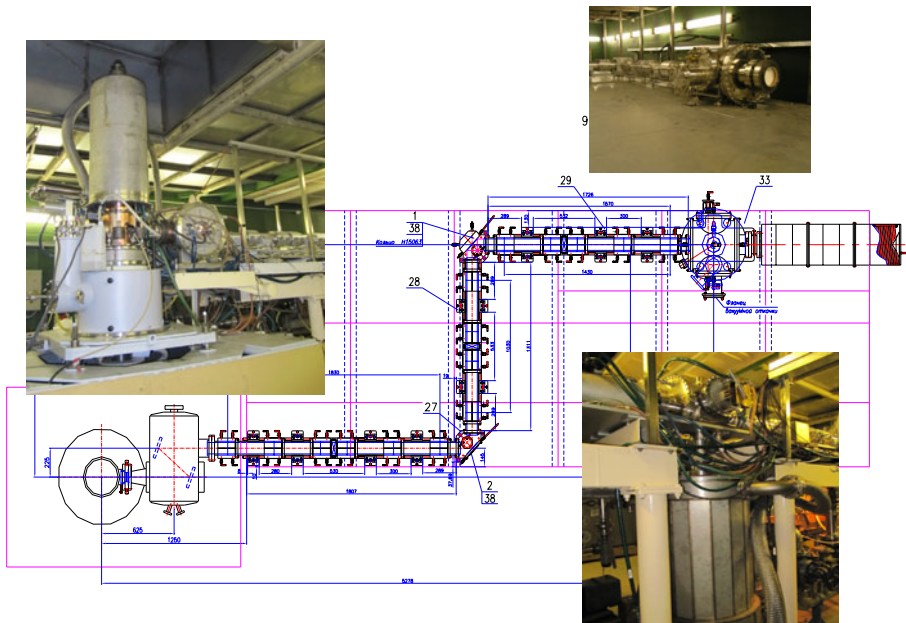


Fig. 5 Schematic of the gyrotron test line. Photos show components of the line: left—gyrotron in cryomagnet, matching optics unit and beginning of the waveguide; right-upper—switch and ceramics window of the short-pulse load; right-low—main stainless steel load for microwaves.

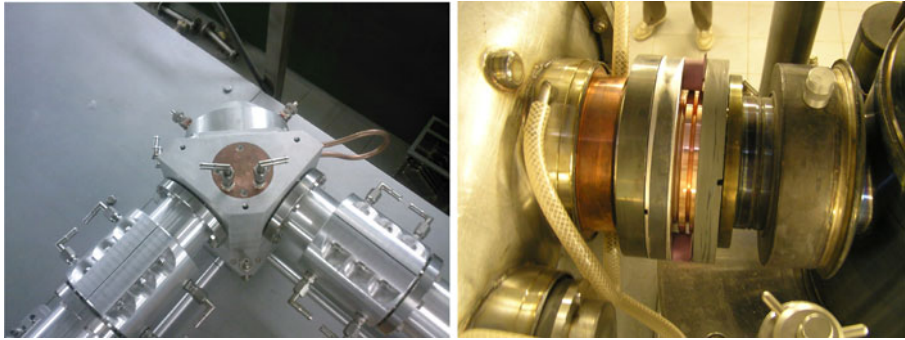


Fig. 6 Components of the line: miter bend with bi-directional coupler (left) and copper bellow between gyrotron and matching optics unit (right).

fundamentally different at higher fields. These problems can be overcome by using high radical concentration and high microwave driving powers. Large signal enhancement can be achieved, even at high fields (9–18 T) if sufficient microwave power (~10 W) is available to drive the polarization transfer. Gyrotrons are the only feasible choice for generating such high microwave powers at high frequencies (100–500 GHz). Here we present the design and test results of a 258.6 GHz transmission line for DNP gyrotron spectrometers. The design of the gyrotron was described previously [9–11].

The transmission line is intended for transmission of 258.6 GHz microwave radiation from the gyrotron (up to 30 Watt in the continuous wave regime) to one of LS or SS DNP spectrometers at the Institut fuer Biophysikalische Chemie Biozentrum of Goethe-Universitaet Frankfurt am Main, Germany. The transmission line includes the following components: quasi-optical mode transducer for conversion of the operating gyrotron mode TE₂₃ into the HE₁₁ mode of the corrugated waveguide transmission line; novel polarizer-attenuator; water flow microwave load with measuring device and amplifier; two-positional power switch; corrugated HE₁₁ Ø18 mm waveguide (160 mm sections); miter bends with directional couplers and detectors (Fig. 8). The Ohmic loss of the HE₁₁ mode in the hard aluminum corrugated waveguide is 0.001 dB/m. These losses are comparable with the 260 GHz microwave absorption in relatively dry 25% humidity air.

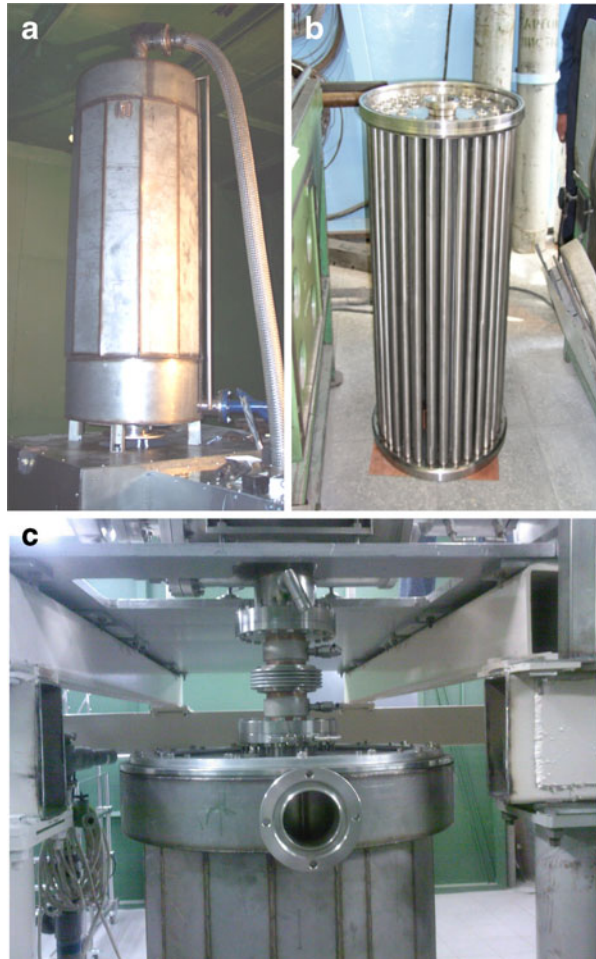
The axial gyrotron output waveguide has a relatively large diameter (20 mm) and thus a small Brillouin angle of the mode. That is the reason, why a simple mode converter without field “pre-shaping” was used. To improve the conversion efficiency from the rotating TE₂₃ mode into the HE₁₁ mode up to 96% specially profiled mirrors were synthesized (Fig. 9). The wave beam has a linear polarization at the output of the mode converter.

The polarizer-attenuator (PA) consists of a miter bend with a grooved rotating mirror and a wire grid in the T-junction of the corrugated waveguides. One shoulder of the junction is connected to the microwave load. Power transmission through the PA depends on the wave beam incidence angle φ and the grooved mirror rotation angle ψ

$$\frac{P_{out}}{P_{in}} = \left(\frac{\cos \varphi \cdot \sin 2\psi}{1 - (\sin \varphi \cdot \cos \psi)^2} \cdot \sin \left(\frac{\delta(\psi)}{2} \right) \right)^2, \tag{4}$$

where $\delta(\psi)$ is a phase shift of TE- and TM-waves after the beam reflection from the corrugated mirror of the polarizer.

Fig. 7 Main water pipe of the 1 MW load with flow of 10 l/sec (a); a version of absorbing stainless steel surface inside the load (b); connection of the load to the waveguide (c).



The $\delta(\psi)$ function was calculated with the integral equation technique. After the polarizer the wave beam with desirable linear polarization penetrates through the thick wire grid of the attenuator into the transmission line.

A simple miter bend with a plane mirror was selected since it provides an allowable diffraction loss of 2% per miter bend. The mechanical switch directs microwaves to one of the SS or the LS spectrometers.

An HE_{11} mode exciter (with WR3 input waveguide) also was developed. Two identical exciters were manufactured and tested. The HE_{11} mode content of $98\pm 1\%$ was obtained from intensity measurements in a few cross sections and phase recovery procedure. An Ohmic loss of 15% in the exciter was measured. The exciter was used, in particular, to calibrate the transmission through the novel polarizer- attenuator at the low power level (Fig. 10).

In experiments with the gyrotron the microwave power was measured by a water-flow calorimeter. The measured HE_{11} mode reflection from the load is about 0.5%. The gyrotron with the load at the straight output operates properly.

Transmission Line structure

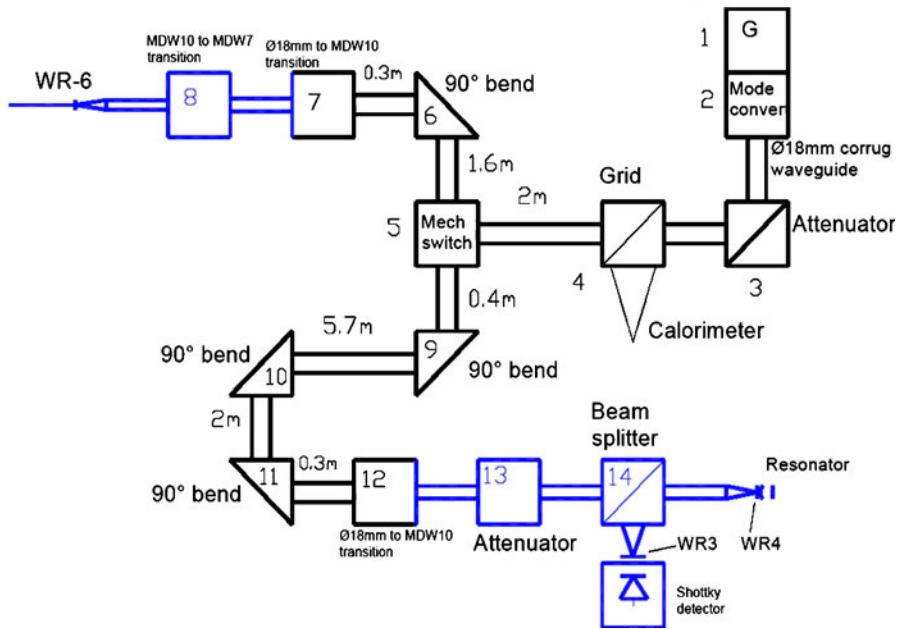
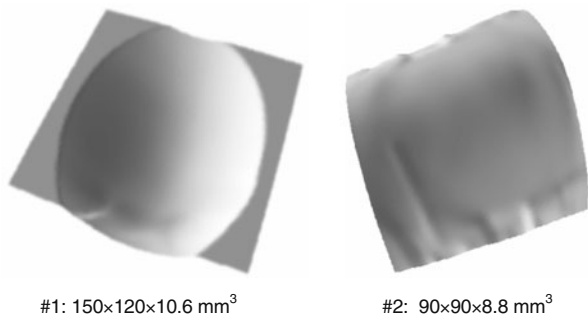


Fig. 8 258 GHz transmission line scheme.

The profiled mirrors of the mode converter were adjusted by use of burn patterns on the paper. During the first hot experiments a standing mode at the gyrotron output was observed. Because of the small caustic of the TE₂₃ mode the wave beams of both rotating modes passed through the converter mirrors. Consequently at the HE₁₁ waveguide two input wave beams separated in space were observed (Fig. 11, a). One of the wave beams was selected for the HE₁₁ mode excitation in the corrugated waveguide. At that stage the second wave beam was lost and absorbed inside the mode converter. The origin of the gyrotron standing mode is under investigation. Burn paper images at the transmission line input and at the LS and SS DNP spectrometers are shown in the Fig. 11 b,c,d.

Output powers of 18–20 W were measured at both input ports of the spectrometers with the water flow load. The HE₁₁ exciters with opposite connection at the WR3 flanges were used as a mode filter to the measure power level in the pure HE₁₁ mode (Fig. 4). The

Fig. 9 Shapes of synthesized mirrors of the quasi-optical mode converter.



#1: 150×120×10.6 mm³

#2: 90×90×8.8 mm³

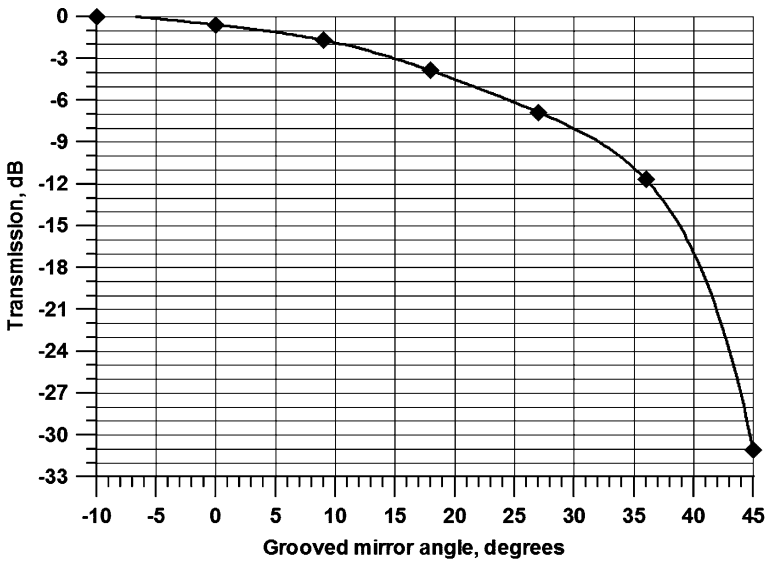


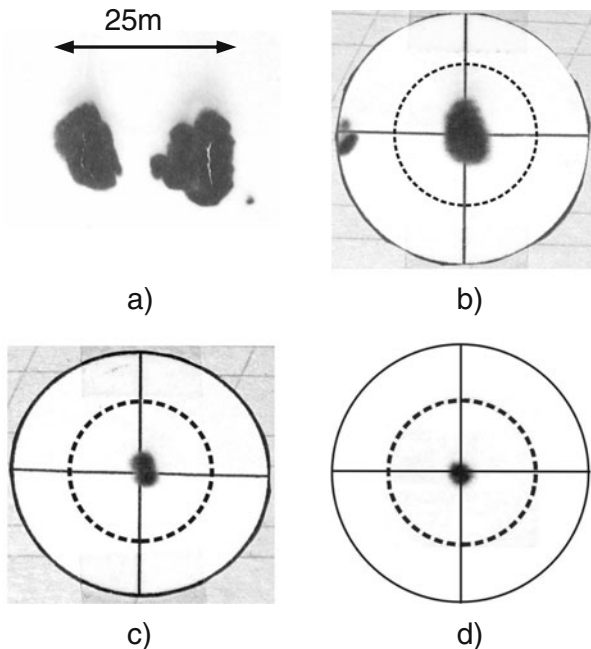
Fig. 10 Measured transmission coefficient through the PA for different grooved mirror angles ψ .

measured microwave power at the spectrometers was about 15 Watt in the pure HE_{11} mode (Fig. 12).

Moreover, the image was burned with the microwave power on the paper and on the wooden slab just after the HE_{11} mode filter (Fig. 13).

The new results in DNP-NMR spectroscopy were obtained with this equipment [12].

Fig. 11 Microwave intensity images on burn paper. **a** after last mirror of the mode converter; **b** one of the beams at the $\varnothing 18$ mm HE_{11} waveguide input; **c** at the SS spectrometer; **d** at the LS spectrometer.



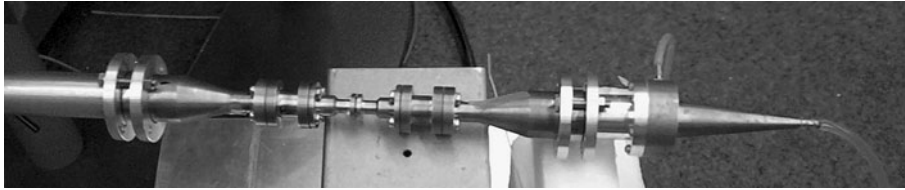


Fig. 12 Mode filter for direct power measurement in the HE_{11} mode at the output ports of the transmission line.

1.4 High-suppression notch filters

To protect the sensitive components of plasma diagnostics systems from powerful gyrotron radiation notch filters are usually used. There is a principal contradiction to provide in a very narrow filter bandwidth of suppression and a high attenuation level. The contradiction can be mitigated in oversized systems. The parameters of the last filter version developed for very high frequencies are shown in Fig. 14. A third waveguide mode is used as the resonant one. Note that there are no other resonances in the 40 GHz band near the operating frequency. The easy mechanical tuning of the central frequency is about 1%.

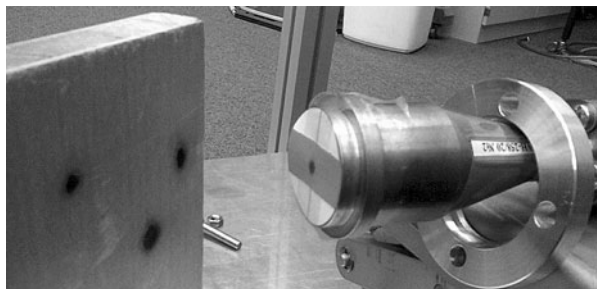
More examples of the filter parameters are shown on Fig. 15.

1.5 Fast laser controlled semiconductor microwave switch

Commutation of powerful microwave flows is an actual problem in modern areas of controlled fusion physics, plasma physics, high resolution coherent spectroscopy, *etc.* The main problem here is to create a fast (nanosecond to microsecond), powerful (from watts up to kW, MW) and high frequency (tens-hundreds of GHz) device for reliable and low-loss switching. The present study is addressed to meet the system of requirements in practice.

Most of the known microwave switches—diodes and transistors, plasma switches, ferrite and microstrip switches only meet these requirements partially. So we consider alternative constructions—quasi-optical or waveguide switches based on high-purity semiconductors. High-purity semiconductors initially demonstrate electro-dynamical properties close to low-loss dielectrics. The process of switching is driven by an optical laser pulse that induces photoconductivity in a small ($\sim 1 \mu\text{m}$) layer near the semiconductor surface. Inducing of photoconductivity and its relaxation are processes with typical times of 1 ns or less for gallium arsenide. The laser driven semiconductor can be built into a resonant (waveguide or quasi-optical) construction to achieve working frequencies up to hundreds of GHz without risk of thermal disruption. The typical power loss in such a device is less than 1%. The

Fig. 13 Burn image at the SS DNP-NMR spectrometer input after HE_{11} mode filter. Microwave power is 15 W.



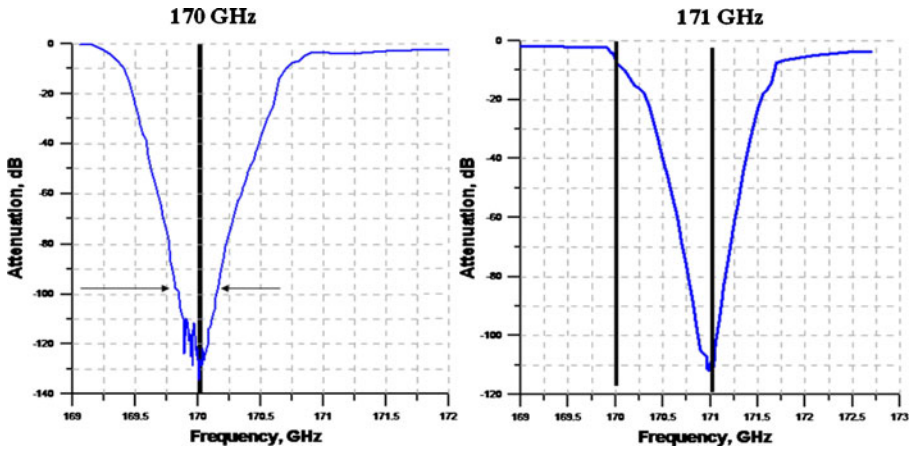


Fig. 14 Suppression of the 170 GHz tunable filter for different frequencies.

target of the presented investigation is to achieve nanosecond level of performance in optically controlled microwave switching. For numerical modeling we use a modified FDTD method. The calculated construction parameters are used to build a real device.

For the calculation of the switch [13] we used a numerical model based on a 2-dimensional finite difference time domain (FDTD, [14]) method for the set of Maxwell’s equations (5). The electric current j (1c) is expressed in terms of total mobility μ of generalized carriers in the semiconductor and their density N :

$$\text{rot}\vec{E} = -\frac{1}{c} \frac{\partial \vec{H}}{\partial t}, \quad \text{rot}\vec{H} = \frac{\varepsilon}{c} \frac{\partial \vec{E}}{\partial t} + \frac{4\pi}{c} \vec{j}, \quad \vec{j} = eN(t, \vec{r})\mu\vec{E}. \quad (5)$$

Here $c=2.998 \cdot 10^{10}$ cm/s is the speed of light in free space, $e=4.8 \cdot 10^{-10}$ CGSE is the electron charge, and $\mu=8.9 \cdot 10^3$ cm²/(V·s) is the total carrier mobility in the semiconductor

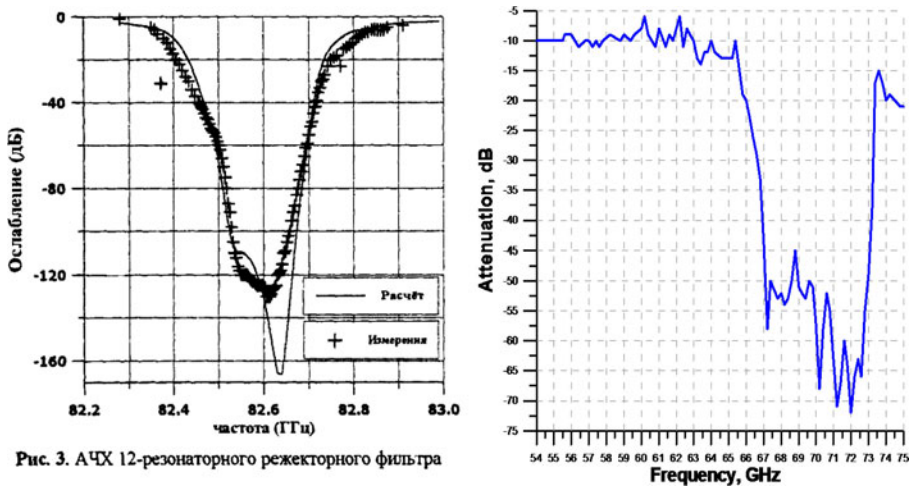


Рис. 3. АЧХ 12-резонаторного режекторного фильтра

Fig. 15 Notch filters: very high-attenuation 82.6 GHz filter based on a single mode waveguide (a); 70 GHz notch filter in an oversized waveguide (7.16×3.58 mm²) for 26–60 GHz EC diagnostic (to protect the system against a 70 GHz gyrotron).

in the case that the electric field is much less than the breakdown field. For calculation of the total carrier density we use the non-stationary modeling equation assuming diffusion, relaxation and induction of photoconductivity by an external optical laser beam pulse:

$$\frac{\partial N}{\partial t} = D\Delta N + g(\vec{r}, t) - G_1(N - N_p). \tag{6}$$

Here $D=28 \text{ cm}^2/\text{s}$ is an ambipolar diffusion coefficient in the semiconductor, $G_1=10^{10} \text{ cm}^{-1}$ is the 1st order (which is the most important) relaxation constant and $N_p=2.1 \cdot 10^6 \text{ cm}^{-3}$ is an equilibrium density rate for pure gallium arsenide at room temperature. At the boundaries of the semiconductor we have no-flow condition $\nabla N=0$. The photo-effect, i.e. the temporal growth of the non-equilibrium carrier density with the laser emission decaying into the depth of the semiconductor, is described as:

$$g(r_{\perp}, t) = I \exp(-\alpha r_{\perp}) \cdot \theta(t - t_0, \tau). \tag{7}$$

The photo-effect constant is expressed as $I = \frac{\alpha W_{pulse} \eta}{S \tau W_{quant}}$, where the reversed emission penetration depth $\alpha=10000 \text{ cm}^{-1}$ corresponds to a typical photoconductivity layer thickness of 1 μm in GaAs for 770 nm optical emission, W_{pulse} is the laser pulse energy, W_{quant} is the laser emission quantum energy, τ is the pulse length, and θ is a step-function. The laser beam area S is 4 mm^2 , η is the efficiency of the photo-effect, its experimental value is 70%.

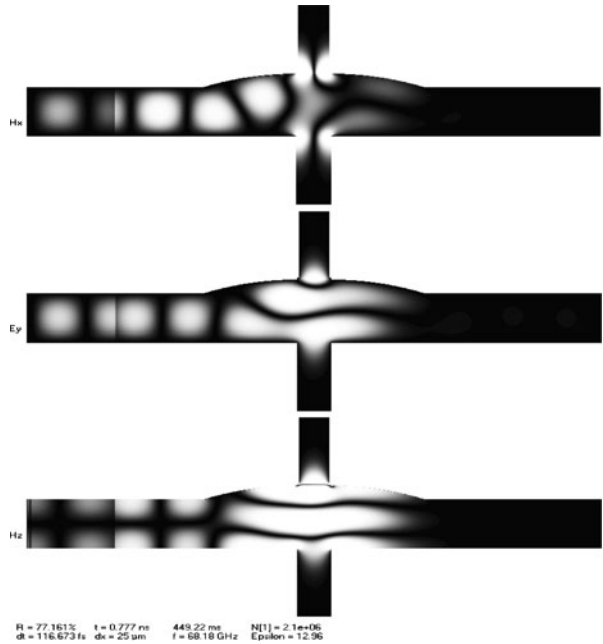
The used modification of the FDTD method includes un-split perfectly matched layer (UPML, [15]) absorbing boundary conditions at the input and output of the modulator, Ohmic losses in metallic walls, and a transparent unidirectional microwave source implied by a 1st order equation. The frequency band of the simulation is set to 50–100 GHz. The spatial step of the computing grid is 0.1 μm for the semiconductor and 25 μm for the other objects—this is sufficient to describe all possible profiles of fields with the photo-effect. The basic temporal grid step is 117 fs, it is automatically adjusted during the simulation to provide adequate description of rapid processes of photoconductivity induction and relaxation. The following picture (Fig. 16) displays a calculation software window with three electromagnetic field component plots (TE-polarization).

At the central parts of the plots, which corresponds to the resonator, we can see a typical “closed” state of the modulator—a resonance of an eigenmode with perfect reflection of the incident wave back to the source. The semiconductor plate is at the base of the upper overcritical vertical waveguide. The resonance can be broken by a laser pulse that induces photoconductivity, so the resonant frequency is “shifted”, the modulator “opens” and the incident wave passes through the modulator without reflection. After the photoconductivity relaxes down to its equilibrium density level, the “closed” state is returned. A typical time of switching between the two states is 1 ns.

Here is a sample photograph (Fig. 17a) of a waveguide semiconductor modulator for 66–72 GHz. It has a gallium arsenide element built in a resonant structure. One can see the microwave output (the input is symmetrical) and the laser input window at the picture. The modulator is controlled by optical laser pulses at the wavelength of 780 nm and with a pulse duration of 100 fs. Each pulse has a typical energy of 10 nJ, the pulse repetition frequency is about 75 MHz. The switched microwave power is 10 mW.

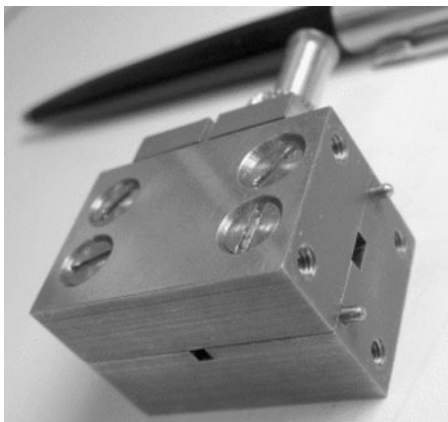
The modulator demonstrates the possibility of a table nanosecond performance operation with low power loss. The following graph (Fig. 17b) shows the detected microwave response from the modulator, the typical times are 200 ps for growth and 1 ns for drop.

Fig. 16 Field components (H_x , E_y , H_z) in the switch resonator without laser illumination.

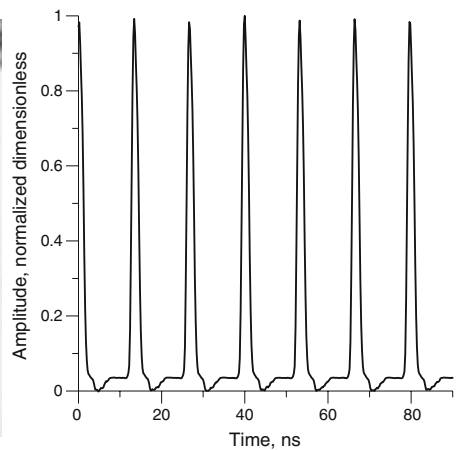


2 Conclusion

The use of multi-mode systems is a necessary approach to handle successfully high-frequency high-power microwaves. In addition multi-mode system provide a possibility to realize features and parameters of transmission line components that are not achievable in single mode waveguides. Analysis and synthesis methods to design such systems are well developed. Various recently developed components are presented in this paper.



a)



b)

Fig. 17 Photo of the cavity with the hole for the laser beam and the tuning plunger (a); transmission coefficient through the modulator when periodic laser pulses illuminate the semiconductor.

Acknowledgement The authors are very grateful to Prof. M. Thumm from KIT Karlsruhe for his detailed discussions of the systems and the support of the present paper.

References

1. M. Thumm, W. Kasperek, “Passive High-Power Microwave Components”, IEEE Trans. Plasma Science, vol. 30, No. 3, June 2002, pp. 755–786.
2. M. Thumm, “Modes and Mode Conversion in Microwave Devices”, in Generation and Application of High Power Microwaves, R.A. Cairns and A.D.R. Phelps, Eds. Bristol, U.K.: IOP, 1996, pp.121–171.
3. B. Z. Katsenelenbaum, Irregular Waveguides with Slowly Varying Parameters (in Russian). Moscow, USSR: Acad. Sci., 1961.
4. D. I. Sobolev, G. G. Denisov, “Principles of Synthesis of Multimode Waveguide Units”, IEEE Transactions on Plasma Science, vol. 38, no. 10, pp. 2825–2830, Oct. 2010.
5. G. G. Denisov, S. V. Samsonov, D. I. Sobolev, “Two-dimensional realization of a method for synthesis of waveguide converters”, Radiophysics and Quantum Electronics, vol. 49, no. 12, pp. 961–967, Dec. 2006.
6. G. G. Denisov, G. I. Kalynova, D. I. Sobolev, “Method for synthesis of waveguide mode converters”, Radiophysics and Quantum Electronics, vol. 47, no. 8, pp. 615–620, Aug. 2004.
7. D.A. Hall, D.C. Maus, G.J. Gerfen, S.J. Inati, L.R. Becerra, F.W. Dahquist and R.G. Griffin. Polarization-Enhanced NMR Spectroscopy of Biomolecules in Frozen Solutions. Science, 276, pp. 930–932, May 1997.
8. L.R. Becerra, G.J. Gerfen, R.J. Temkin, D.J. Singel, and R.G. Griffin. Dynamic nuclear polarization with a cyclotron resonance maser at 5T. Physical Review Letters, 71(21), pp. 3561–3564, November 1993.
9. V. Bajaj *et al.* 250 GHz CW gyrotron oscillator for DNP in biological solid state NMR, Journal of Magnetic Resonance, 189, pp. 251–279, 2007.
10. Zapevalov, V.E., Dubrov, V.V., Fix, A.Sh., Kopelovich, E.A., Kufin, A.N., Malygin, O.V., Manuilov, V. N., Zavolsky, N.A. Development of 260 GHz second harmonic CW gyrotron with high stability of output parameters for DNP spectroscopy (2009) 34th Int. conf. IRMMW-THz 2009.
11. N. Zavolsky, V. Zapevalov, O. Malygin, M. Moiseev, A. Sedov Optimization of the cavity of a second-gyroharmonic continuous-wave gyrotron with an operating frequency 258 GHz Radiophysics and Quantum Electronics, Vol. 52, No. 5. (1 May 2009), pp. 379–385.
12. V. Denysenkov, M. J. Prandolini, M. Gafurov, B. Endeward, and T. F. Prisner, Phys. Chem. Chem. Phys., 2010, 12, 5786–5790.
13. M. L. Kulygin, G. G. Denisov, V. V. Kocharovskiy. Modeling of dynamic effects in a laser-driven semiconductor switch of high-power microwaves. Journal of infrared, millimeter and terahertz waves, Vol. 31, Issue 1 (2010), p. 31.
14. A.Taflove. Computational electrodynamics: the finite-difference time-domain method. Boston MA: Artech House, 1995.
15. S. D. Gedney. An anisotropic perfectly matched layer—absorbing medium for the truncation of FDTD lattices. IEEE Trans. Antennas and Propagation, vol. 44, No. 12, Dec 1996, pp. 1630–1639.